# Glass Transition Temperature and Density Scaling in Cumene at Very High Pressure

T. C. Ransom[1,2,*] and W. F. Oliver[2]
[1]Naval Research Laboratory, Chemistry Division, Code 6100, Washington DC 20375-5342, USA
[2]Physics Department, University of Arkansas, Fayetteville, Arkansas 72701, USA
(Received 2 May 2016; revised manuscript received 5 May 2017; published 14 July 2017)

We present a new method that allows direct measurements of the glass transition temperature $T_g$ at pressures up to 4.55 GPa in the glass-forming liquid cumene (isopropylbenzene). This new method uses a diamond anvil cell and can measure $T_g$ at pressures of 10 GPa or greater. Measuring $T_g$ at the glass → liquid transition involves monitoring the disappearance of pressure gradients initially present in the glass, but also takes advantage of the large increase in the volume expansion coefficient $\alpha_p$ at $T_g$ as the supercooled or superpressed liquid is entered. Accurate $T_g(P)$ values in cumene allow us to show that density scaling holds along this isochronous line up to pressures much higher than any previous study, corresponding to a density increase of 29%. Our results for cumene over this huge compression range yield $\rho^\gamma/T = C$, where C is a constant and where $\gamma = 4.77 \pm 0.02$ for this nonassociated glass-forming system. Finally, high-pressure cumene viscosity data from the literature taken at much lower pressures and at several different temperatures, corresponding to a large dynamic range of nearly 13 orders of magnitude, are shown to superimpose on a plot of $\eta$ vs $\rho^\gamma/T$ for the same value of $\gamma$.

DOI: 10.1103/PhysRevLett.119.025702

Many liquids and polymers are readily cooled well below their freezing temperature $T_m$, exhibiting a dramatic increase of viscosity $\eta$ and slowing down of structural relaxation time $\tau_\alpha$ by many orders of magnitude upon approach to the glass transition temperature $T_g$, marked by $\eta = 10^{13}$ poise and $\tau_\alpha = 100$ s [1]. Though several theoretical approaches exist [2–8], a consensus for a microscopic description for this behavior remains elusive, and hence Anderson's comment in 1995 that understanding the nature of glass and the glass transition is probably "the deepest and most interesting unsolved problem in solid state theory" [9] remains valid today. In addition to the traditional approach of glass formation by supercooling, it is also possible to achieve vitrification through superpressing, where densification drives the transition [10]. Any ultimate fundamental solution of the glass transition problem must describe phenomena associated with both pathways. Variable temperature and pressure depolarized light scattering showed more than 20 years ago that $\tau_\alpha$ is not driven by density alone; instead, it is controlled by the same combination of $T$ and $P$ (or $T$ and $\rho$) as is viscosity [11]. Soon afterward, variable pressure quasielastic neutron scattering results gave intriguing hints of a scaling relation valid near the crossover line $P_c(T)$ in which glass transition dynamics are governed by a constant parameter proportional to $\rho^4/T$ for the van der Waals fragile glass-forming liquid *o*-terphenyl [12]. Subsequent studies discovered that many glass-forming systems obey the more general scaling relation

$$x(\rho, T) = F(\rho^\gamma/T), \tag{1}$$

where $x$ is $\tau_\alpha$ or $\eta$, $F$ is an unknown function, and $\gamma$ is a material-dependent scaling exponent [10,13–18]. This scaling, known as density scaling, allows dynamic measurements taken over a broad range of $T$ and $\rho$ to collapse onto a single master curve when plotted versus $\rho^\gamma/T$.

Density scaling also allows researchers to construct isochoric plots or calculate isochoric derivatives and, thus, compare the relative importance of $\rho$ and $T$ independently [19–21], whereas isobaric cooling experiments always entangle both quantities via thermal contraction. It has helped lead to the classification of certain liquids as "strongly correlating" and the development of isomorph theory in which many properties of correlating liquids are invariant under conditions of constant $\rho^\gamma/T$ [22–24]. Furthermore, the exponent $\gamma$ is theorized to provide a critical quantitative connection between cooperative dynamics and the intermolecular potential [20,25,26]. Though this scaling behavior has been found to hold over broad dynamic ranges, most tests of Eq. (1) in glass-forming systems to date have been limited to pressures up to about 1 GPa and, hence, relatively small compression ranges. This limitation has led to debate about whether the scaling variable truly requires a power law in density or if an alternative function such as one linear in density $(\rho - \rho^*)/T$, where $\rho^*$ is a material constant, might equally suffice [10]; small density ranges have made it difficult to answer this question [19]. There is also recent computational evidence that power-law scaling breaks down in the high-density limit [27], a result that can only be tested experimentally at very high pressures. A powerful approach to test Eq. (1) over broad density ranges is by measuring the $P$ dependence of $T_g$.

The $T_g(P)$ boundary represents an isochronous line at $\tau_\alpha(\rho_g, T_g) \approx 100$ s. For constant $\tau_\alpha$, Eq. (1) requires the constraint

 

$$C = \rho_g^{\gamma}/T_g, \quad (2)$$

where $C$ is a constant along the $T_g(P)$ line. In this Letter, we present the first direct measurements of $T_g(P)$ using a new technique in a high-pressure diamond anvil cell (DAC). These measurements were performed on the glass-forming liquid cumene up to $P = 4.55$ GPa. We find that Eq. (2) describes the data extremely well, yielding a value of $\gamma$ that holds over the entire pressure range corresponding to a compression of 29%. Furthermore, we take all known temperature and pressure-dependent viscosity data for cumene, corresponding to a dynamic range of 13 orders of magnitude, and show that these data collapse onto a single curve when plotted versus $\rho^{\gamma}/T$ for the same value of $\gamma$.

The technique for measuring $T_g(P)$ is based upon the combination of two well-known properties associated with the glass transition. First, a liquid exhibits hydrostatic conditions, whereas compression of a glass leads to a nonuniform stress distribution, manifested by pressure gradients across the sample [28–30]. In a DAC, pressure is measured via fluorescence spectra [31] from small ruby chips placed in different locations in the sample chamber, thereby measuring the pressure in various regions. By establishing pressure gradients across a sample in the glass state, and then slowly heating the sample, $T_g$ is determined as the temperature at which the pressure gradients vanish. A schematic of this process is shown in Fig. 1. Isobaric lines show a possible initial state and evolution of stress with increasing temperature. Initial pressure gradients established at low temperature continually decrease upon heating until hydrostatic conditions are reached above $T_g$.

To further improve accuracy, an additional technique was used based upon the significant increase in the thermal expansivity $\alpha_P$ at $T_g$ when heating into the liquid state. Other pressure-volume-temperature experiments have made use of this property to measure $T_g$ through a slope change in isobaric $V$ vs $T$ curves, but mostly at quite modest pressures [26,32,33], with a few notable exceptions up to 1–2 GPa [16,34]. A DAC is composed of two opposing diamond anvils, which form the top and bottom of the sample chamber, and a cylindrical hole drilled into a metal gasket forms the side walls as shown in Fig. 1. Pressure is easily measured in a DAC, whereas volume is not. When making large temperature changes, precise control of volume or pressure is not possible because of the thermal expansion of the sample, gasket, diamond anvils, and steel anvil holders. However, a slope change is still manifest at $T_g$ in the $P$ vs $T$ plot, which provides another good marker of the glass transition. This slope change occurs since $\alpha_P$ increases above $T_g$ and the viscous liquid sample expands against the diamonds and gasket walls to a much greater degree than when in the glassy state. With the combination of the two techniques, determination of $T_g$ at high pressure in a DAC is quite accurate.

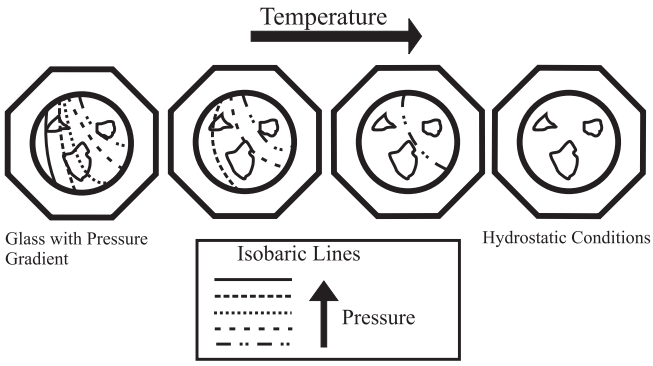


FIG. 1. Schematic glass → liquid transition sequence showing possible initial pressure gradient lines in the DAC sample at low $T$ evolving upon heating until hydrostatic conditions are reached above $T_g$. Octagonal boundary represents diamond culets (tips of the diamonds), and the smaller circular region represents the sample contained within the steel gasket hole. Three shapes represent rubies at different locations.

Cumene (isopropylbenzene) [$C_6H_5CH(CH_3)_2$ $T_m$ = 177 K, $T_g(1\ \text{atm}) = 127 \pm 2$ K MW = 120.10 g/mol, purity > 99%] was obtained from Sigma-Aldrich and used as is. It is a good glass former and exhibits an intermediate isobaric fragility $m_P = 70$ at 1 atm [35–37]. It was loaded into a Merrell-Bassett–style DAC with a culet size of 500 $\mu$m. Stainless steel was used as the gasket material. Ruby fluorescence was used for pressure measurements, and an argon-ion 514.5-nm laser line was used as an excitation source. Fluorescence spectra were obtained with a 0.5-m Jarrel-Ash spectrometer and fit according to the method described in Ref. [38], enabling sub-Å resolution and pressure uncertainty of about ±0.03 GPa. Custom furnace and cryogenic systems were used in the high- and low-temperature regimes. For each measurement, temperature was initially lowered and then pressure was increased until large differences of at least 0.1 GPa were present between the locations of the three rubies. Temperature was then increased in a stepwise fashion, initially with jumps of 10–15 °C every 30 min when the sample was far from the glass transition, and then in steps of 1–2 °C every 15 min close to $T_g$. By incrementing $T$ in this manner, pressure gradients eventually vanish (within uncertainty), after which heating steps were continued for at least another 20 °C. The system was then cooled well below $T_g$, pressure was increased, and the sample was allowed to equilibrate before beginning the next run.

Four typical heating runs spanning the pressure range of the experiment are shown in Fig. 2. Each starts with pressure differences of 0.2–0.6 GPa at low temperatures in the glassy state. With increasing temperature, the region of highest pressure consistently decreases, while the ruby or rubies at lower pressure show weaker pressure variation as visible in ruby 3 of Figs. 2(a) and 2(b). The pressure gradient across the sample decreases until it eventually vanishes (within uncertainty), and hydrostatic conditions are achieved. Coincident with the loss of gradients is a

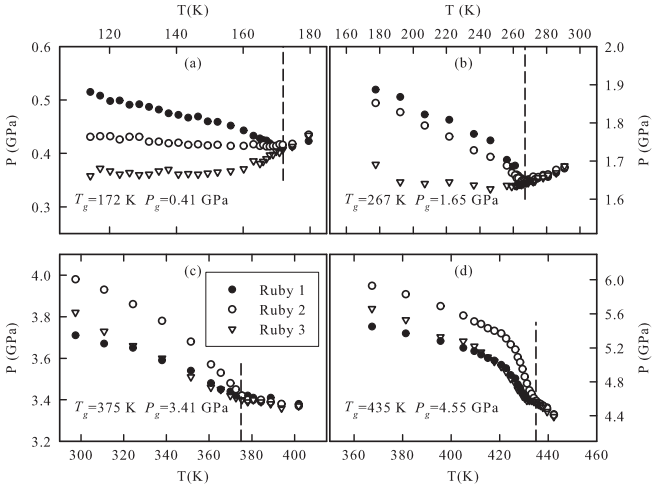


FIG. 2. Four representative glass → liquid transition heating runs. Pressure measurements were obtained from the three rubies arbitrarily designated 1, 2, and 3, as indicated in the legend in the lower right. Runs (a) and (b) were taken with one DAC loading, while (c) and (d) were obtained with a second DAC loading.

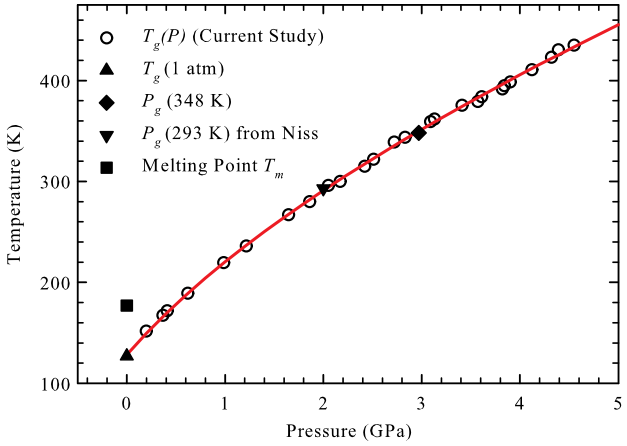


FIG. 3. $T_g$ data obtained from 26 heating runs (circle). Atmospheric pressure value $T_g(1\text{atm}) = 127 \pm 2$ K (upward filled triangle) is an average of measurements from several sources [39–41]. Atmospheric pressure melting temperature (filled square) is from Ref. [40]. Value of $P_g(348\text{ K})$ (filled diamond) was obtained from Ref. [43]. Value of $P_g(293\text{K})$ (downward filled triangle) was obtained from Ref. [42]. Solid line shows fit to Eq. (3).

marked increase in the slope $dP/dT$, most dramatic in the ruby initially at the highest pressure. In the low-temperature runs [Figs. 2(a) and 2(b)], this slope actually changes from negative to positive, showing an increasing pressure for $T > T_g$. Combining the two markers of pressure gradient disappearance and an increase in $dP/dT$, we obtain measurements of the thermodynamic conditions at the glass transition ($T_g$, $P_g$), with estimated uncertainties ($T_g \pm 4$ K, $P_g \pm 0.05$ GPa). Values of $T_g$ so determined are shown as vertical dashed lines in Fig. 2.

The resulting values of $T_g$ thus obtained are shown in Fig. 3 from 26 such heating runs. In the limit of low pressure, the data show excellent agreement with $T_g(1\text{ bar}) = 127 \pm 2$ K (upward filled triangle) determined from the average value of several differential thermal analysis experiments [39–41]. Comparison with dynamic measurements show good agreement near room temperature with an estimation of $P_g(293\text{ K}) \approx 2$ GPa (downward filled triangle) by Niss [42], who used the high-pressure viscosity data of Li *et al.* [11]. Finally, there is excellent agreement with $P_g(348\text{K}) = 2.97$ GPa (filed diamond), determined as the pressure at which $\tau_\alpha(P_g) = 100$ s from high-pressure depolarized light-scattering measurements of $\tau_\alpha$ along an isotherm at 75 °C [43]. Strong agreement with both calorimetric and dynamic measurements is good evidence that the current technique is able to measure $T_g$ quite accurately over the very large pressure range of this study. We fit the $T_g(P)$ data, including the estimation of $T_g(1\text{ bar}) = 127$ K, to the much used Andersson-Andersson equation [44],

$$T_g(P) = T_{g0}\left(1 + \frac{b}{c}P\right)^{1/b}, \tag{3}$$

where $T_{g0}$ is the glass transition temperature at atmospheric pressure, and $b$ and $c$ are fitting parameters. A fit of Eq. (3), shown as the solid line in Fig. 3, describes the data quite well over the entire range, with $T_{g0} = 129 \pm 2$ K, $b = 1.67 \pm 0.04$, and $c = 1.16 \pm 0.05$ GPa. The $T_g(P)$ curve corresponds, to a good approximation, to an isochronous line, and should provide dynamic studies of cumene at high pressure with a solid estimation of $\tau_\alpha = 100-1000$ s or $\eta = 10^{13}$–$10^{14}$ poise at $T_g$ (or $P_g$) [45]. This will reduce the need for such studies to extrapolate, typically by many orders of magnitude, to $T_g$, which gives large uncertainty to calculated quantities such as fragility [46], and obfuscates any correlated trends or other conclusions drawn.

Our accurate measurements of $T_g(P)$ enable the isochronous testing of density scaling up to extremely high pressures using Eq. (2). The scaling exponent $\gamma$ is found from the slope of a plot of $\log_{10} T_g$ vs $\log_{10} \rho_g$ shown in the inset of Fig. 4. In order to construct such a plot, a Tait equation of state (EOS) was used based upon measurements by Bridgman up to 4 GPa (see Appendix). An excellent linear relationship is indeed evident up to 4.55 GPa, giving no indication that Eq. (2) breaks down at high densities, at least over the range explored here. A linear fit yielded a slope of $\gamma = 4.77 \pm 0.02$. This value is comparable to those found for other nonassociated glass-forming liquids [26]. While Eq. (2) predicts $T_g \propto \rho^\gamma$, Dreyfus *et al.* pointed out in Ref. [15] that over limited density ranges it was difficult to differentiate this power-law prediction from other alternatives such as a linear form $T_g \propto \rho - \rho^*$ or a model based on free-volume theory $T_g \propto \rho/(\rho_0 - \rho)$, where $\rho_0$ is a fitting parameter

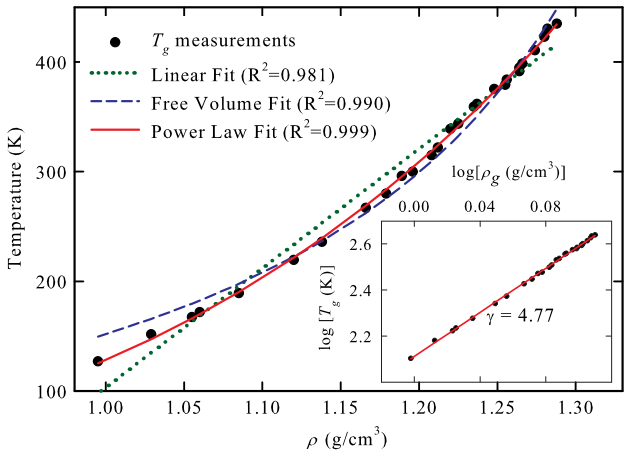


FIG. 4. Plot of $T_g$ vs $\rho_g$ with fits to three models discussed in the text. Inset: Plot of $\log_{10} T_g$ vs $\log_{10} \rho_g$ with linear fit.

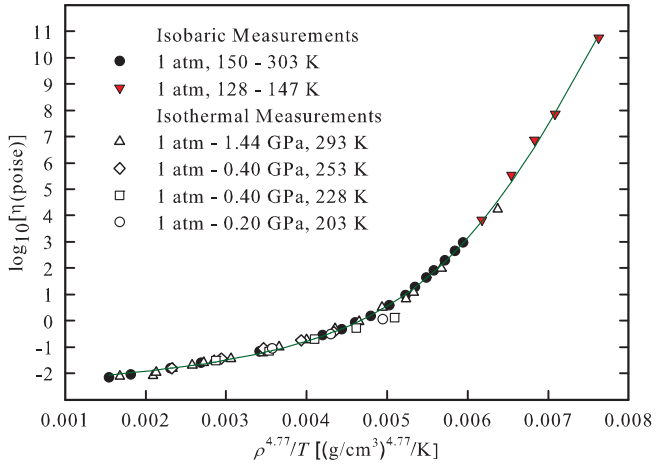


FIG. 5. Plot of $\log_{10}\eta$ vs $\rho^{4.77}/T$ with atmospheric pressure viscosity data from Ref. [35] (filled circle) and Ref. [36] (filled downward triangle). High pressure isothermal data were obtained from Ref. [11] for 293 K (triangle), and from Ref. [47] for 253 K (diamond), 228 K (square), and 203 K (circle). Solid line is fit to Eq. (10) from Ref. [17].

representing a particular high-density value. It is thus illustrative to plot $T_g$ vs $\rho_g$ and compare fits to these three functions, shown in Fig. 4. Clearly, all three functions can follow general trends of the data (particularly over small compression ranges); however, only the power-law prediction is able to describe these data accurately over the full density range covered in this study.

The exponent $\gamma$ found from the linear fit to $\log_{10} T_g$vs $\log_{10}\rho_g$ is typically determined by collecting $\eta$ or $\tau_\alpha$ data taken under various thermodynamic conditions, and then iteratively guessing at values of $\gamma$ until the data superimpose when plotted vs $\rho^\gamma/T$. To test our value of $\gamma$ from $T_g(P)$ data, we collected previous $\eta$ measurements from various sources under isothermal and isobaric conditions. Isobaric $\eta$ measurements were obtained at 1 atm in Ref. [35] down to 150 K and in Ref. [36] down to 130 K, covering a huge dynamic range of 13 orders of magnitude. High-pressure isothermal measurements of $\eta$ up to 0.4 GPa were obtained at 203, 228, and 253 K in Ref. [47], and up to 1.4 GPa at 293 K in Ref. [11]. These data sets are all plotted versus $\rho^{4.77}/T$ in Fig. 5, where all are found to superimpose in agreement with Eq. (1), noting that the same scaling exponent $\gamma = 4.77$ from the isochronous $T_g(P)$ analysis was used. Similar results were also reported in Ref. [42] with $\gamma = 4.85$ found from the iterative superposition method.

In summary, direct measurements of $T_g(P)$ using a powerful new method are presented for the glass-forming liquid cumene to pressures up to 4.55 GPa. These data are used for an isochronous density scaling analysis yielding the scaling exponent $\gamma = 4.77 \pm 0.02$. Comparison of several alternative scaling models revealed that only the power-law form accurately describes data over this very large compression range of 29%. A density scaling check was then performed with all published viscosity data in cumene at various temperatures and pressures yielding excellent superposition of all data with the same value of $\gamma$. Hence, the nonassociated liquid cumene is well described by a single scaling parameter over its full dynamic range and over a thermodynamic range heretofore unexplored.

We gratefully acknowledge fruitful discussions with Pradeep Kumar, Mike Roland, Riccardo Casalini, and Adam Holt. Financial support was provided from the National Science Foundation Division of Materials Research, the Ray Hughes Fellowship, and the University of Arkansas Honors College.

## APPENDIX: EQUATION OF STATE

Bridgman measured the compression of cumene up to 4 GPa at room temperature [48]. Cibulka and Takagi [49] later combined these measurements with other data and fit them with a Tait EOS to model the pressure-dependent density,

$$\rho(T,P) = \frac{\rho_0(T)}{1 - C(T)\ln\left(\frac{B(T)+P}{B(T)+0.0001\ \text{GPa}}\right)}, \qquad \text{(A1)}$$

where $C(T)$ and $B(T)$ are temperature-dependent parameters which drive the EOS, and $\rho_0(T)$ is the atmospheric pressure density. The range of temperature for this EOS given in Ref. [49] is quite restricted, from only 298 to 333 K; thus, to better approximate the parameters $C(T)$ and $B(T)$, we borrowed their temperature dependence from toluene (also given in Ref. [49]), which is structurally quite similar to cumene, and has data over a much larger temperature range, from 179 to 583 K. From the toluene EOS, the parameter $B(T)$ was increased by 0.007 GPa to overlap with that of cumene in its range, yielding

$$B(T) = \sum_{i=0}^{4} b_i [(T - T_0)/100]^i$$

$$T_0 = 298.15\text{K} \quad \text{and} \quad \vec{b} = \begin{bmatrix} 0.111102\ \text{GPa} \\ -0.080954\ \text{GPa K}^{-1} \\ 0.0226\ \text{GPa K}^{-2} \\ -0.0034\ \text{GPa K}^{-3} \\ 0.00028\ \text{GPa K}^{-4} \end{bmatrix}. \tag{A2}$$

Also, $C(T)$ has a linear dependence for toluene, with a nearly identical value to that of cumene in the 298–333 K range, so it was borrowed with a 20% reduction of the slope $dC/dT$ so that the high-temperature behavior of $\alpha_P$ had a more physical pressure dependence, $C(T) = 0.093736 - 0.8[(0.005004\ K^{-1})(T - T_0)/100]$.

*timothy.ransom.ctr@nrl.navy.mil


[1] C. A. Angell, Formation of glasses from liquids and biopolymers, Science **267**, 1924 (1995).

[2] G. Adam and J. H. Gibbs, On the temperature dependence of cooperative relaxation properties in glass-forming liquids, J. Chem. Phys. **43**, 139 (1965).

[3] D. Turnbull and M. H. Cohen, On the free-volume model of the liquid-glass transition, J. Chem. Phys. **52**, 3038 (1970).

[4] M. H. Cohen and G. S. Grest, A new free-volume theory of the glass transition, Ann. N.Y. Acad. Sci. **371**, 199 (1981).

[5] P. G. Debenedetti and F. H. Stillinger, Supercooled liquids and the glass transition, Nature (London) **410**, 259 (2001).

[6] W. Götze, *Complex Dynamics of Glass-Forming Liquids: A Mode-Coupling Theory*, International Series of Monographs on Physics Vol. 143 (Oxford University Press, New York, 2008).

[7] L. Berthier and G. Biroli, Theoretical perspective on the glass transition and amorphous materials, Rev. Mod. Phys. **83**, 587 (2011).

[8] L. Berthier and M. D. Ediger, Facets of glass physics, Phys. Today **69**, No. 1 40 (2016).

[9] H. Weintraub, M. Ashburner, P. N. Goodfellow, H. F. Lodish, C. Arntzen, P. Anderson, T. Rice, T. H. Geballe, A. R. Means, H. M. Ranney *et al.*, Through the glass lightly, Science **267**, 1615 (1995).

[10] C. M. Roland, S. Hensel-Bielowka, M. Paluch, and R. Casalini, Supercooled dynamics of glass-forming liquids and polymers under hydrostatic pressure, Rep. Prog. Phys. **68**, 1405 (2005).

[11] G. Li, H. E. King Jr, W. F. Oliver, C. A. Herbst, and H. Z. Cummins, Pressure and Temperature Dependence of Glass-Transition Dynamics in a "Fragile" Glass Former, Phys. Rev. Lett. **74**, 2280 (1995).

[12] A. Tölle, H. Schober, J. Wuttke, O. G. Randl, and F. Fujara, Fast Relaxation in a Fragile Liquid Under Pressure, Phys. Rev. Lett. **80**, 2374 (1998).

[13] R. Casalini and C. M. Roland, Thermodynamical scaling of the glass transition dynamics, Phys. Rev. E **69**, 062501 (2004).

[14] G. Tarjus, D. Kivelson, S. Mossa, and C. Alba-Simionesco, Disentangling density and temperature effects in the viscous slowing down of glassforming liquids, J. Chem. Phys. **120**, 6135 (2004).

[15] C. Dreyfus, A. Le Grand, J. Gapinski, W. Steffen, and A. Patkowski, Scaling the $\alpha$-relaxation time of supercooled fragile organic liquids, Eur. Phys. J. B **42**, 309 (2004).

[16] S. Pawlus, R. Casalini, C. M. Roland, M. Paluch, S. J. Rzoska, and J. Ziolo, Temperature and volume effects on the change of dynamics in propylene carbonate, Phys. Rev. E **70**, 061501 (2004).

[17] R. Casalini and C. M. Roland, Scaling of the supercooled dynamics and its relation to the pressure dependences of the dynamic crossover and the fragility of glass formers, Phys. Rev. B **71**, 014210 (2005).

[18] R. Casalini, S. S. Bair, and C. M. Roland, Density scaling and decoupling in o-terphenyl, salol, and dibutyphthalate, J. Chem. Phys. **145**, 064502 (2016).

[19] C. Alba-Simionesco, A. Cailliaux, A. Alegria, and G. Tarjus, Scaling out the density dependence of the $\alpha$ relaxation in glass-forming polymers, Europhys. Lett. **68**, 58 (2004).

[20] R. Casalini, U. Mohanty, and C. M. Roland, Thermodynamic interpretation of the scaling of the dynamics of supercooled liquids, J. Chem. Phys. **125**, 014505 (2006).

[21] C. Alba-Simionesco and G. Tarjus, Temperature versus density effects in glassforming liquids and polymers: A scaling hypothesis and its consequences, J. Non-Cryst. Solids **352**, 4888 (2006).

[22] T. B. Schrøder, N. Gnan, U. R. Pedersen, N. P. Bailey, and J. C. Dyre, Pressure-energy correlations in liquids. V. Isomorphs in generalized Lennard-Jones systems, J. Chem. Phys. **134**, 164505 (2011).

[23] U. R. Pedersen, N. Gnan, N. P. Bailey, T. B. Schrøder, and J. C. Dyre, Strongly correlating liquids and their isomorphs, J. Non-Cryst. Solids **357**, 320 (2011).

[24] T. S. Ingebrigtsen, T. B. Schrøder, and J. C. Dyre, What is a Simple Liquid?, Phys. Rev. X **2**, 011011 (2012).

[25] A. Grzybowski, M. Paluch, K. Grzybowska, and S. Haracz, Communication: Relationships between Intermolecular potential, thermodynamics, and dynamic scaling in viscous systems, J. Chem. Phys. **133**, 161101 (2010).

[26] K. Koperwas, A. Grzybowski, K. Grzybowska, Z. Wojnarowska, J. Pionteck, A. P. Sokolov, and M. Paluch, Pressure coefficient of the glass transition temperature in the thermodynamic scaling regime, Phys. Rev. E **86**, 041502 (2012).

[27] L. Bøhling, T. S. Ingebrigtsen, A. Grzybowski, M. Paluch, J. C. Dyre, and T. B. Schrøder, Scaling of viscous dynamics in simple liquids: theory, simulation and experiment, New J. Phys. **14**, 113035 (2012).

[28] G. J. Piermarini, S. Block, and J. D. Barnett, Hydrostatic limits in liquids and solids to 100 kbar, J. Appl. Phys. **44**, 5377 (1973).

[29] R. G. Munro, S. Block, and G. J. Piermarini, Correlation of the glass transition and the pressure dependence of viscosity in liquids, J. Appl. Phys. **50**, 6779 (1979).

[30] S. Klotz, J. Chervin, P. Munsch, and G. Le Marchand, Hydrostatic limits of 11 pressure transmitting media, J. Phys. D **42**, 075413 (2009).

[31] G. J. Piermarini, S. Block, J. D. Barnett, and R. A. Forman, Calibration of the pressure dependence of the R1 ruby fluorescence line to 195 kbar, J. Appl. Phys. **46**, 2774 (1975).
[32] M. Paluch, Effect of temperature, pressure and volume on long time relaxation dynamics in fragile glass-forming liquid, J. Chem. Phys. **115**, 10029 (2001).
[33] Z. Wojnarowska, M. Paluch, A. Grzybowski, K. Adrjanowicz, K. Grzybowska, K. Kaminski, P. Wlodarczyk, and J. Pionteck, Study of molecular dynamics of pharmaceutically important protic ionic liquid-verapamil hydrochloride. I. Test of thermodynamic scaling, J. Chem. Phys. **131**, 104505 (2009).
[34] M. S. Elsaesser, I. Kohl, E. Mayer, and T. Loerting, Novel method to detect the volumetric glass → liquid transition at high pressures: glycerol as a test case, J. Phys. Chem. B **111**, 8038 (2007).
[35] A. J. Barlow, J. Lamb, and A. J. Matheson, Viscous behaviour of supercooled liquids, Proc. R. Soc. A **292**, 322 (1966).
[36] A. C. Ling and J. E. Willard, Viscosities of some organic glasses used as trapping matrixes, J. Phys. Chem. **72**, 1918 (1968).
[37] L. Wang, C. A. Angell, and R. Richert, Fragility and thermodynamics in nonpolymeric glass-forming liquids, J. Chem. Phys. **125**, 074505 (2006).
[38] R. G. Munro, G. J. Piermarini, S. Block, and W. B. Holzapfel, Model line-shape analysis for the ruby R lines used for pressure measurement, J. Appl. Phys. **57**, 165 (1985).
[39] M. R. Carpenter, D. B. Davies, and A. J. Matheson, Measurement of the glass-transition temperature of simple liquids, J. Chem. Phys. **46**, 2451 (1967).
[40] G. P. Johari and M. Goldstein, Viscous liquids and the glass transition. II. Secondary relaxations in glasses of rigid molecules, J. Chem. Phys. **53**, 2372 (1970).
[41] S. S. N. Murthy, S. K. Nayak *et al.*, Novel differential scanning calorimetric studies of supercooled organic liquids, J. Chem. Soc., Faraday Trans. **89**, 509 (1993).
[42] K. Niss, Ph.D. thesis, Universite Paris-Sud, 2007.
[43] T. C. Ransom, W. F. Oliver, and K. Lyon (unpublished).
[44] S. P. Andersson and O. Andersson, Relaxation studies of poly (propylene glycol) under high pressure, Macromolecules **31**, 2999 (1998).
[45] Because the time scales for these experiments are on the order of a few minutes, $T_g$ values thus determined may be better described by a larger $\tau_\alpha$ or $\eta$ value.
[46] S. Pawlus, M. Paluch, J. Ziolo, and C. M. Roland, On the pressure dependence of the fragility of glycerol, J. Phys. Condens. Matter **21**, 332101 (2009).
[47] I. Artaki and J. Jonas, Pressure effect on the coupling between rotational and translational motions of supercooled viscous fluids, J. Chem. Phys. **82**, 3360 (1985).
[48] P. W. Bridgman, Further rough compressions to 40,000 Kg/cm$^2$, especially certain liquids, Proc. Am. Acad. Arts Sci. **77** 129 (1949).
[49] I. Cibulka and T. Takagi, $P$-$\rho$-$T$ data of liquids: summarization and evaluation. 5. Aromatic hydrocarbons, J. Chem. Eng. Data **44**, 411 (1999).